information

Article

Evaluation of 60 GHz Wireless Connectivity for an Automated Warehouse Suitable for Industry 4.0 †

Rahul Gulia *, Abhishek Vashist, Amlan Ganguly *, Clark Hochgraf and Michael E. Kuhl

Rochester Institute of Technology, 1 Lomb Memorial Dr., Rochester, NY 14623, USA; av8911@rit.edu (A.V.); cghiee@rit.edu (C.H.); mekeie@rit.edu (M.E.K.)

* Correspondence: rg9828@rit.edu (R.G.); axgeec@rit.edu (A.G.)

† This article is a revised and expanded version of a paper entitled "Evaluation of Wireless Connectivity in an Automated Warehouse at 60 GHz", which was presented at the Proceedings of the 2022 IEEE International Conference on Consumer Electronics 566 (ICCE), Las Vegas, NV, USA, 7–9 January 2022; pp. 1–6.

Abstract: The fourth industrial revolution focuses on the digitization and automation of supply chains resulting in a significant transformation of methods for goods production and delivery systems. To enable this, automated warehousing is demanding unprecedented vehicle-to-vehicle and vehicle-to-infrastructure communication rates and reliability. The 60 GHz frequency band can deliver multi-gigabit/second data rates to satisfy the increasing demands of network connectivity by smart warehouses. In this paper, we aim to investigate the network connectivity in the 60 GHz millimeter-wave band inside an automated warehouse. A key hindrance to robust and high-speed network connectivity, especially, at mmWave frequencies stems from numerous non-line-of-sight (nLOS) paths in the transmission medium due to various interacting objects such as metal shelves and storage boxes. The continual change in the warehouse storage configuration significantly affects the multipath reflected components and shadow fading effects, thus adding complexity to establishing stable, yet fast, network coverage. In this study, network connectivity in an automated warehouse is analyzed at 60 GHz using Network Simulator-3 (NS-3) channel simulations. We examine a simple warehouse model with several metallic shelves and storage materials of standard proportions. Our investigation indicates that the indoor warehouse network performance relies on the line-of-sight and nLOS propagation paths, the existence of reflective materials, and the autonomous material handling agents present around the access point (AP). In addition, we discuss the network performance under varied conditions including the AP height and storage materials on the warehouse shelves. We also analyze the network performance in each aisle of the warehouse in addition to its SINR heatmap to understand the 60 GHz network connectivity.

Keywords: automated warehouse; industry 4.0; 60 GHz propagation models; SINR heatmaps

Citation: Gulia, R.; Vashist, A.; Ganguly, A.; Hochgraf, C.; Kuhl, M.E. Evaluation of 60 GHz Wireless Connectivity for an Automated Warehouse Suitable for Industry 4.0. *Information* **2023**, *14*, 506. https://doi.org/10.3390/info14090506

Academic Editor: Ruggero Lanotte

Received: 2 August 2023
Revised: 11 September 2023
Accepted: 13 September 2023
Published: 15 September 2023

1. Introduction

The fourth industrial revolution, often referred to as industry 4.0, envisions a technological transformation in industries, primarily centered around automated manufacturing. This transformation encompasses automated material handling, facilitated by smart interconnections among components, and the integration of artificial intelligence (AI) into production facilities. Erboz [1] highlights the potential for enhancing efficiency in smart industries through self-monitoring systems. The convergence of machinery and the internet of things (IoT) empowers smart industries to autonomously analyze and diagnose issues within their operations. In the context of a smart warehouse, this entails the integration of multiple IoT sensors with automated forklifts, drones, and other mobile devices. To realize this fundamental shift in smart industrial environments, innovative wireless connectivity is imperative. Such connectivity should offer high bandwidth, flexibility, intelligence, speed, security, and low latency. Effective connectivity is pivotal across the entire supply chain,

from production stations to customer orders, encompassing warehousing and delivery. It plays a pivotal role in ensuring the seamless delivery of consumer goods. Consequently, to enhance the operational efficiency of a warehouse, robust wireless connectivity is a prerequisite for the successful transition from a human-operated warehouse to an automated one.

Sophisticated path planning models have been developed to enhance the performance of autonomous material handling agents (AMHAs) within intricate warehouse environments, with the aim of improving delivery systems, as referenced in [2,3]. AMHAs represent autonomous forklifts or vehicles employed in smart warehouses, specifically designed for efficient material transport within various warehouse sections. When these transport vehicles, known as AMHAs, are operational in a smart warehouse, they are tasked with autonomous navigation. This entails the meticulous detection, prediction, tracking, and planning of paths, particularly in the presence of other autonomous vehicles operating in close proximity, as discussed in [4,5]. Such coordination requires extensive information exchange among AMHAs, necessitating the presence of robust wireless connectivity, as emphasized in [6].

The Federal Communications Commission (FCC) has designated an unlicensed spectrum ranging from 57 to 64 GHz for wireless communications. Within this 60 GHz millimeter-wave (mmWave) band, there exists significant potential for delivering exceptionally high speeds and robust channel capacity, catering to line-of-sight (LOS) as well as nLOS applications. The remarkable performance attributes of the 60 GHz band make it well suited to meet the connectivity demands of smart warehouses, thereby enhancing the performance of AMHAs and facilitating secure multi-tasking operations. Deployed alongside advanced antenna systems, this band leverages its distinctive propagation characteristics, including high oxygen absorption, excellent immunity to interference, heightened security, and frequency reuse, as elucidated in [7]. However, it is worth noting that mmWave frequency bands are susceptible to increased penetration and diffraction losses compared to lower frequency bands. Consequently, directional transmission becomes a critical feature within the 3rd Generation Partnership Project (3GPP) 5G new radio (NR) standard. In response, 3GPP has redesigned the antenna systems for mmWave frequency bands, with a focus on beam management, as detailed in [8,9], as well as beam measurement to support directional communication, as discussed in [10]. The intrinsic characteristics of the 60 GHz band, coupled with these advancements, make it capable of delivering a high quality of service (QoS) in smart industrial environments that rely on numerous machine-to-machine (M2M) communications and IoT sensors.

In response to the limitations observed in prior studies, we present a comprehensive examination of network performance within an automated warehouse specifically operating at the 60 GHz frequency band. Warehouses are characterized by a substantial presence of metallic shelves, leading to wireless propagation behavior that significantly contrasts with that observed in residential or office environments [11]. In this study, we integrate 60 GHz indoor channel models into the NS-3 simulator, while also considering penetration losses associated with diverse building materials, as outlined in [12]. Our warehouse simulation involves concrete walls and metal shelves stocked with materials like wood and glass. This setup allows us to thoroughly assess network performance by examining signal reflection characteristics within the aisles. Notably, to the best of our knowledge, the exploration of 60 GHz Wi-Fi connectivity in the context of a smart warehouse, as discussed in this paper, represents a pioneering contribution to the existing literature.

The contributions of this paper are summarized as follows:

- Our investigation focuses on evaluating wireless network connectivity within the 60 GHz frequency band in a smart warehouse. To achieve this, we made modifications to NS-3, enabling the incorporation of appropriate propagation losses characteristic of the 60 GHz indoor environment.
- The metric we employ to assess network connectivity is the signal to interference and noise ratio (SINR). Notably, due to the significant presence of multipath components

emanating from the metal shelves, we found that nLOS-propagated signals exhibit comparable performance to LOS-propagated signals.

- We conducted an in-depth examination of network performance in the context of higher offered loads, considering the presence of multiple AMHAs in dynamic environments. Our analysis encompasses mean throughput and delay measurements for both LOS and nLOS scenarios, specifically taking into account the multipath components introduced by metallic structures.
- Furthermore, we explored the influence of varying AP heights on network performance to understand the impact of multipath components.
- Our investigation also scrutinized the impact of different storage materials, namely, wood and glass, on network performance. Notably, we observed that the network exhibited superior SINR performance with glass due to the lower penetration loss associated with this material.
- To gain a more comprehensive understanding, we visualized the SINR distribution throughout the entire warehouse using heatmaps. This visualization revealed a smoother SINR transition from LOS path aisles to nLOS path aisles.
- In conclusion, we analyzed key parameters including mean SINR, standard deviation of SINR, and changes in SINR when an AMHA transitioned from the primary LOS aisle to any nLOS aisle within the warehouse models under consideration. Our findings demonstrate the presence of a stable 60 GHz network in the warehouse, even with various shelf configurations.

The remainder of this paper is organized as follows. Section 2 surveys the related work. Section 3 discusses the environment description and the measurement procedures and processing. The design of the simulation platform is reported in Section 4. The results are presented and analyzed in Section 5, with the conclusions and future work in Section 6.

2. Related Work

Channel modeling serves as a foundational element in the design of efficient wireless communication systems, and there has been notable research activity in this realm at the 60 GHz frequency band. One noteworthy endeavor involved obtaining real-world data through the use of a 60 GHz channel sounder to explore the application of the multiple-input multiple-output (MIMO) technique within indoor environments, as documented in [13]. The enhancement in multi-hop indoor wireless connectivity was achieved through the implementation of a diversity reception scheme, as discussed in [14]. Another innovative approach leveraged the physical characteristics of the uniform planar array (U-PA) and 2-dimensional discrete Fourier transform (2D-DFT) to introduce a novel channel estimation scheme tailored for 60 GHz massive MIMO systems, as outlined in [15]. Effectively transmitting multi-gigabit-per-second (Gb/s) customer data within a 60 GHz indoor communication system involved the application of various modulation schemes, as detailed in [16]. Furthermore, network performance within the 60 GHz frequency band was investigated in a smart warehouse context, without human intervention. This encompassed a comprehensive study of multipath components originating from metallic structures and various storage materials surrounding the access points (APs) and AMHAs, as elucidated in [17]. They conducted an extensive investigation into multipath components to discern the influence of metal frames within this dynamic network context, drawing comparisons between the 60 GHz and 5 GHz bands. However, this work does not demonstrate connectivity with fine-grained heatmaps.

In [18], channel characteristics were studied in a real warehouse environment at 2.4 GHz and 868 MHz to guarantee flexible and reliable connectivity in dynamic large-scale industrial applications, especially for connected warehouses. In [19], a 5G system architecture in smart factories was presented, focusing on ultra-reliable use cases at 28 GHz and 60 GHz. The study included channel modeling, ray tracing simulations, and a frequency comparison to highlight the potential of 60 GHz channels for reliable communication in industrial settings.

In [20], the manuscript delves into the propagation characteristics at 60 GHz within indoor environments, employing the shooting and bouncing ray tracing/image (SBR/IM) method. In [21], the analysis encompasses both LOS and nLOS scenarios, addressing omni-directional path loss models and received power. Furthermore, a propagation measurement campaign at 60 GHz was conducted within an indoor office setting, leveraging a vector network analyzer (VNA) to exploit multipaths generated by various indoor elements, such as people, furnishings, and obstructions. In [22], the study encompasses 60 GHz channel sounding and throughput measurements, focusing on nLOS path characteristics in an indoor residential environment. In [23], the investigation extends to studying outdoor-to-indoor (O2I) penetration losses for frequencies ranging from 28 GHz to 73 GHz across various scenarios, utilizing the NYUSIM model. It scrutinizes the impact of diverse building materials (including glass, wood, IRR glass, and concrete) and antenna properties in O2I scenarios. In [24], for indoor-to-indoor and O2I scenarios, an office building was utilized to analyze penetration losses across different incident angles, underscoring the substantial penetration loss experienced by a 60 GHz channel in indoor environments. Additionally, in [25], the terragraph sounder (TG) channel sounder tool, developed by META, serves as a practical instrument for measuring physical channel properties. The investigations conducted encompass both LOS and nLOS scenarios, evaluating path loss and signal-to-interference-plus-noise ratio (SINR). To enhance the understanding of indoor propagation, a ray tracing simulator was discussed, leading to the creation of a data-driven indoor propagation model for multiple frequencies, as described in [26]. This model was subsequently employed with a convolutional encoder–decoder to predict path loss in uncharted areas of indoor environments.

While there is a substantial body of literature on 60 GHz channel models in indoor settings, most of it focuses on irregular environments like offices or homes. As industrial automation continues to expand, our goal is to investigate the potential of the 60 GHz frequency band in automated warehouses. Warehouses typically have large number of metallic shelves causing very different wireless propagation behavior compared to residential or office spaces. The existing literature lacks a comprehensive analysis of the 60 GHz channel model and its suitability for warehouse environments, hindering the transition to automated warehouses that require multi-gigabit network connectivity. To address this gap, we conduct a study that considers the effects of widely used materials, such as metal, wood, and glass, in a warehouse with an isotropic antenna system. This analysis is conducted without the influence of massive MIMO technology. Furthermore, in smart warehouses, AMHAs are expected to autonomously navigate by detecting, predicting, tracking, and planning paths in the presence of other autonomous vehicles nearby. This will necessitate extensive information sharing among AMHAs, highlighting the critical need for reliable wireless connectivity.

3. Wireless Connectivity in Automated Warehouses

Detailed information about the characteristics of the simulated warehouse model is presented in the subsequent subsections. These sections provide comprehensive coverage of the dimensions of the shelves and storage materials, as well as the positions of the APs and AMHAs, all of which are essential for the exploration of both the LOS and nLOS scenarios. Additionally, we delve into the procedure implemented to assess the performance of the 60 GHz network within the smart warehouse.

3.1. Propagation Environment

Figure 1 provides a top-view representation of the NS-3 simulated automated warehouse, illustrating the positions of the AP and AMHAs. The warehouse possesses dimensions of 55 × 60 × 16 m (length × width × height), with the AP situated on the ceiling at a height of 15 m from the ground. The AMHAs, crucial for analyzing LOS and nLOS paths' impacts on network performance, are positioned at a height of 1 meter from the ground. It is worth noting that our simulated warehouse environment intentionally excludes the modeling of a human presence. This decision aligns with our research objective, which

focuses on investigating the performance of the 60 GHz network within a fully automated warehouse setting.

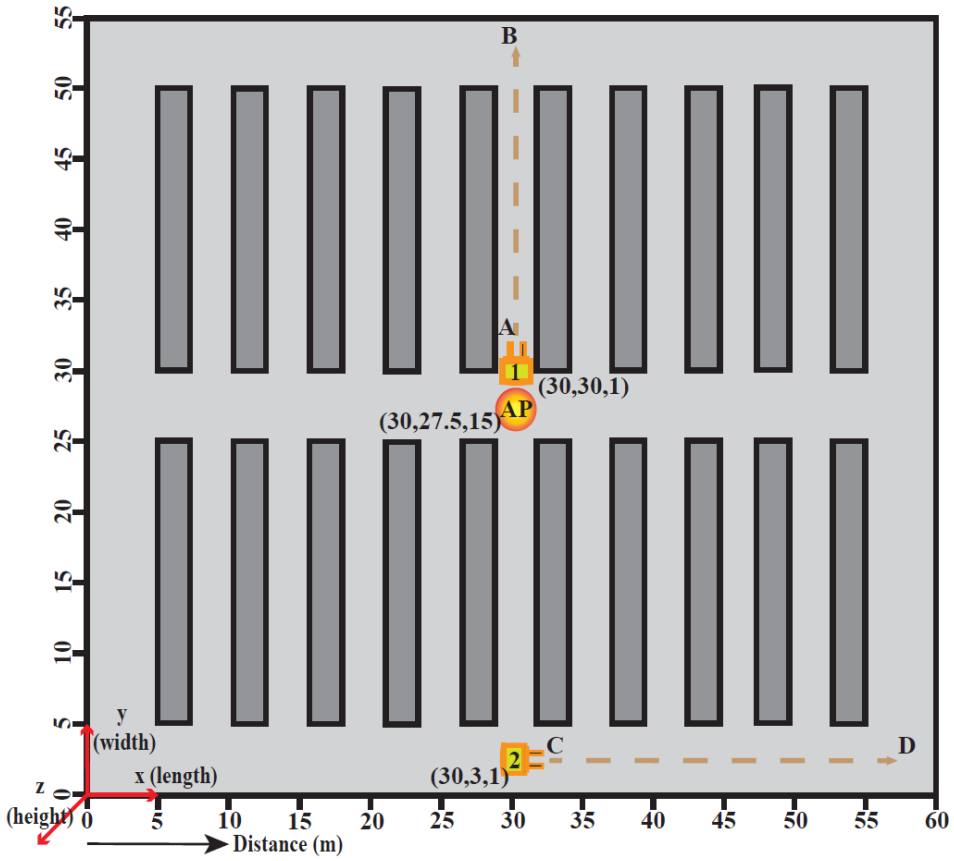

Figure 1. Automated warehouse model used to analyze LOS and nLOS propagation characteristics showing the location of AP and AMHA-1 and -2's initial positions, A and C, respectively. B and D denote AMHA final positions

In our NS-3 simulated warehouse model, we have constructed concrete walls with a thickness of 0.2 m, and there are no windows incorporated into these walls. To thoroughly investigate the impact of multipath components on the wireless network, we have strategically positioned 20 metal racks within the warehouse. These racks are equipped with either wood or glass as storage materials. Each rack has dimensions of 2.3 × 20 × 14 m, as detailed in [27]. To ensure efficient movement of the AMHAs in the aisles and expedite order processing, we have placed the racks with a separation of 3 meters between them. Furthermore, we have maintained a distance of 5 m between the warehouse walls and the shelves to facilitate the smooth movement of AMHAs in the corners of the warehouse. In our modeling approach, we have positioned the pillars within the automated warehouse in close proximity to the shelves. This consideration allows us to focus solely on reflections originating from the metal shelves in the various case studies that we are investigating.

3.2. Measurement Procedure and Processing

We conducted measurements using point-to-point (P2P) wireless communication at the 60 GHz frequency band. The setup involved transmitting signals from a fixed AP to a mobile receiver (Rx). The AMHAs were positioned at a height of 1 m above the ground. This arrangement allowed us to investigate propagation characteristics both with a single AMHA and in scenarios involving multiple AMHAs. The AMHA was programmed to move at a consistent speed of either 2 m per second or 5 m per second, simulating the operation of a forklift within an automated warehouse while maintaining a safe speed, as detailed in [28]. Our investigation encompassed a range of case studies aimed at

analyzing the impact of LOS- and nLOS-propagated paths on the 60 GHz wireless network, particularly in the presence of metal racks. The simulated model comprised the elements of the warehouse, including its building walls, metal racks, wooden storage blocks, glass storage blocks, AMHAs, and an AP. These elements were implemented within the NS-3 framework using various classes provided by the *Building* module.

4. Design of Simulation Platform

The primary objective of this study is to explore the impact of varying load levels on key network metrics, specifically, mean throughput and mean delay. To achieve this, we strategically positioned AMHAs at different locations within the warehouse. While these AMHAs remained stationary, they operated at random speeds, enabling us to comprehensively analyze network performance across different scenarios. Furthermore, we conducted investigations into the influence of AP heights on AMHA performance, with a specific focus on both LOS and nLOS propagation scenarios. To deepen our analysis, we substituted wooden shelf storage materials with glass and examined their effects on SINR performance. We then carried out a comprehensive SINR distribution analysis within the automated warehouse, including the generation of SINR heatmaps with APs positioned at a height of 15 m. This allowed us to closely scrutinize the impact of multipath components on the 60 GHz network. Additionally, we investigated SINR variations within each warehouse aisle, enabling us to generalize the simulated results for a range of shelf configurations. This involved a thorough examination of key SINR metrics, encompassing mean SINR, SINR standard deviation, and changes in SINR as the AMHA transitioned from the primary LOS aisle to any nLOS aisle within the 16 m warehouse models.

4.1. Simulation Architecture

NS-3 stands as an open-source discrete-event network simulator that serves as a valuable research tool for addressing performance-related queries in computer networking. Simulation is frequently employed in wireless research endeavors, primarily due to the substantial costs associated with 5G network analyzers and real-time experimentation setups. Attempting to replicate results across different testbed sites or at various times can be challenging due to shifting conditions. In accordance with the 5G NR standards proposed by the Third Generation Partnership Project (3GPP) [29], the NS-3 has integrated a mmWave module, thereby enabling end-to-end communication at mmWave frequencies [12]. This module relies on a stochastic channel model, which has been seamlessly incorporated into NS-3 for the purpose of evaluating 5G network performance, as documented in [30,31].

The 3GPP adopted a stochastic channel model (SCM) to evaluate the 5G NR, which has been integrated with NS-3 [29]. This SCM was developed to support large-scale antenna arrays and to accommodate a wide frequency range of up to 100 GHz. It models a channel matrix $\mathbf{H}_{u,s}(t,\tau)$, with each entry corresponding to the channel impulse response between the sth antenna element of the base station (BS) and the uth antenna element of the user terminal (UT) at delay τ at time t. $\mathbf{H}_{u,s}(t,\tau)$ is generated by the superposition of N different clusters, each representing the multipath signals that arrive and/or depart the BS and UT antenna elements with certain angles (azimuth and zenith). The 3GPP 5G NR proposed the number of clusters (N) to be 15 for LOS and 19 for nLOS scenarios in an indoor office environment [29]. Each cluster is a result of 20 rays coupled together for both azimuth and zenith angles. An LOS cluster, if present between BS and UT, will be modeled with the strongest power and minimum delay. The nLOS clusters represent the reflection and scattering from various wooden, glass, and metallic objects present in an environment.

The SCM simulation flow is shown in Figure 2. Each instance of an SCM $\mathbf{H}_{u,s}(t,\tau)$ is generated by the combination of large-scale and small-scale fading parameters. Parameters like delay spread (DS), angular spreads (arrival and/or departure of azimuth and elevation angles), the Rician K factor (K), and shadow fading (SF) are taken into consideration while generating the large-scale parameters for different BS-UT links, along with small-scale fading parameters like cluster delays.

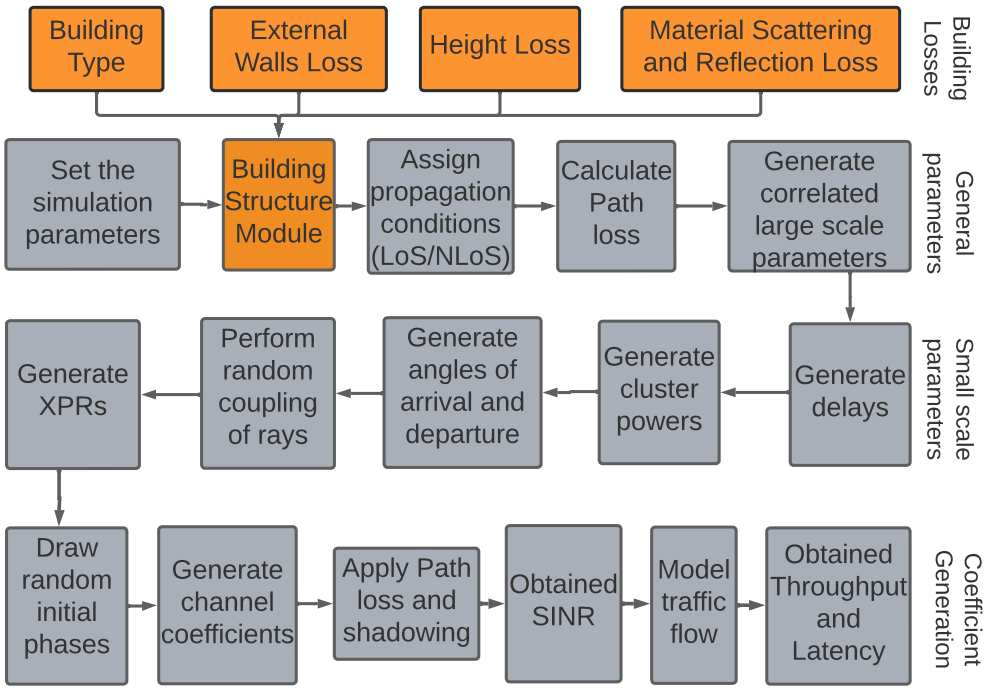

Figure 2. Simulation flow adapted for this paper. Colored blocks represent this paper's contributions.

Within NS-3, the building structure module takes on the role of generating the propagation loss model for in-building scenarios. In Figure 2, the colored blocks denote the additional components necessary to account for losses stemming from different types of building materials. This module includes a *Building* class responsible for modeling the building in a simulated 5G NS-3 scenario. It encompasses various parameters such as building type, building wall material type, the number of rooms, and the number of floors. Building type options can be specified as *Residential*, *Office*, or *Commercial*, while wall materials can be defined as *Wood*, *ConcreteWithWindows*, *ConcreteWithoutWindows*, and *StoneBlocks*. Additionally, the building module features a *MobilityBuildingInfo* class, which maintains information about the BS and UT nodes within the building. The *BuildingsPropagationLossModel* class calculates the total loss within a building as a unified component, taking into account the positions of the BS and UT. This class is also responsible for introducing shadowing effects, encompassing penetration, reflection, and scattering losses incurred due to various objects interacting along different paths between the nodes.

To augment the comprehensiveness of our research, we conducted a comparative analysis between the path loss heatmaps generated by NS-3 and those produced by the ray tracing analysis using the EM DeepRay simulator [26] at 2.6 GHz frequency. The path loss for an indoor environment inside a room of dimensions 300 dm $\times$ 850 dm is evaluated using our proposed NS-3 based simulation platform and is visually presented in Figure 3. Compared with the exact same indoor environment in [26], the proposed simulation achieves a a high accuracy with similar shadow and reflection effects.

Our proposed approach within NS-3 is capable of simulating the impact of metal within an indoor environment, effectively incorporating both reflective and scattering effects. In our method operating at 60 GHz, we observed a substantial disparity in network performance when compared to the 5 GHz frequency band [17], particularly in LOS and nLOS scenarios. Hao Xu, et al. [11], have noted that potent reflectors can yield robust nLOS signals, surpassing the strength of LOS signals. Remarkably, we observed analogous behavior within our simulated indoor environment.

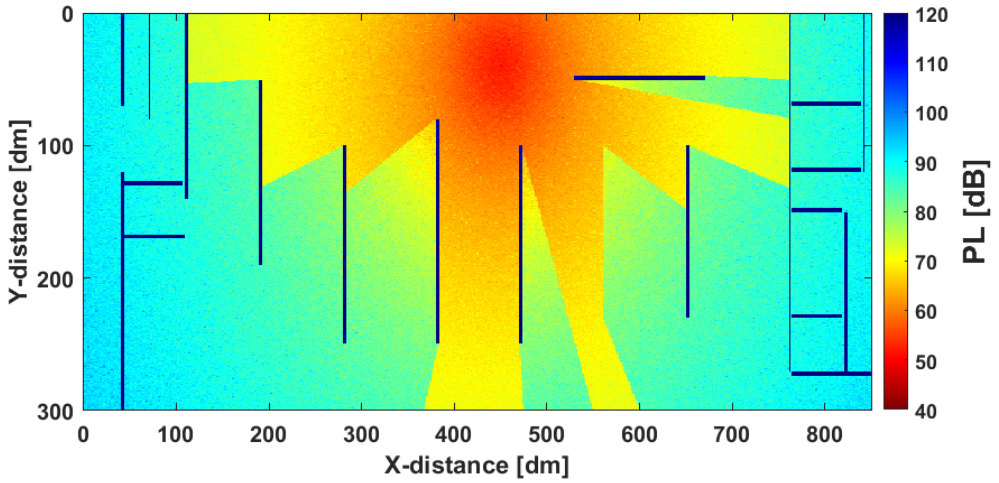

Figure 3. Path loss (PL) heatmap simulated through the proposed NS-3 platform.

4.2. Simulation of 60 GHz Propagation Model

A detailed study was performed on the 60 GHz indoor path loss models [11]. To conduct the measurement campaign, a vector network analyzer or a sliding correlator was used to analyze the path loss in a 60 GHz indoor environment. The model was created for a particular site with metal stud walls, substantially attenuating the 60 GHz propagated signals. The indoor environment channel model encountered most of the loss from the metal studs present in the walls near the Tx and Rx. A considerable amount of transmission power propagated to the Rx through the dominant LOS path and from a few strong first-order reflections [32]. This model was incorporated into the NS-3 modules to simulate a realistic automated warehouse environment that takes the reflections from the surrounding metallic structures into consideration. To support the 5 GHz indoor environments, the NS-3 simulator incorporates the COST-231 Okumara model (Equation (4.4.3) in the COST-231 final report), propagation loss from the Tx and Rx heights, and the Tx–Rx distance. This model was used to compare with the simulated 60 GHz smart warehouse model.

Shadow fading effects encompass the signal power fluctuations received from diverse objects in the vicinity of the Tx and Rx nodes. These fluctuations arise due to scattering and reflections occurring at interacting objects, thereby introducing variations in the propagation environment's multipath components. Consequently, these fluctuations have a notable impact on the transmitted signal. Within NS-3, the *BuildingsPropagationLossModel* class is employed to introduce a range of shadow fading effects from the indoor environment into the propagated channel model. This class also incorporates additional path loss model elements that are contingent on the building's characteristics, including external wall loss/penetration loss (EWL), internal wall loss (IWL), and height gain (HG). In conjunction with these effects already present in the existing NS-3 module, we have integrated an additional loss component into the indoor channel model. This new component accounts for scattering and reflection losses originating from metallic objects within the indoor environment.

The 60 GHz frequency band indoor environment was investigated to study the reflections from the metallic structures placed in the measurement campaign [33]. An HP 8510C vector analyzer was employed to experiment with the presence of three aligned metallic cabinets placed in the center of the room under investigation. Both LOS and nLOS path scenarios were studied to analyze their effects on the indoor channel model. The multipath reflective signals contributed dominantly to the 60 GHz channel model in an indoor environment, thus making it a suitable match for our scenario. The automated warehouse model under investigation was simulated in NS-3 with 20 metal shelves, resulting in a higher scattering and reflective environment. The model developed in [33] was included in the *MaterialScatteringReflectionLoss()* function in the *BuildingsPropagationLossModel*

class to incorporate the additional scattering loss from these metal cabinets. As given in Equation (1), the normalized received power (NRP) was defined as

$$NRP_d[dB] = NRP(d_o) - 10\ nlog\left(\frac{d}{d_o}\right) + \mathcal{X}_\sigma \quad (1)$$

where $NRP(d_o)$ is the NRP at reference distance d_o, d is the Tx–Rx distance, n is the path loss exponent, and $\mathcal{X}_\sigma$ is the zero-mean Gaussian distributed random variable with the standard deviation σ. NRPs are defined for LOS and nLOS separately using the fitted curves. The parameters were derived at different transmitter heights [33].

To compare the simulated 60 GHz indoor environment channel characteristics with those of the 5 GHz channel model, we modified the NS-3 module to incorporate the scattering and reflection loss from the metallic structures at 5 GHz. The reflection and scattering losses from various metal studs in the walls around the office were developed for the 5 GHz channel model [34]. The measurement campaign was conducted in a shielded room containing metallic walls and doors with the AP placed in the center of the room. As described above, we used this model in the *MaterialScatteringReflectionLoss()* function in *BuildingsPropagationLossModel()* class to add the metal scattering and reflection losses from the metal racks placed in the warehouse for a 5 GHz channel model.

4.3. 60 GHz Penetration Loss

The accuracy of an indoor path loss model stems from the understanding of the multipath propagation mechanism. The effects of interacting objects in an indoor environment play a crucial role in strengthening the propagation of the transmitted power to the Rx. The nLOS-propagated signals will dominate the stochastic channel model (SCM) response in a high multipath indoor scenario. The abundance of metal shelves in an automated warehouse gives rise to a scatter-rich indoor environment, but the literature survey lacks an analysis of the 60 GHz frequency band and its losses in an automated warehouse environment. The 60 GHz band suffers from high penetration losses and may pass the Rx undetected, and thus, demands a detailed study of these losses to design an accurate end-to-end system simulation.

The NS-3 *Building* module incorporates the propagation models for various scenarios in and around the vicinity of a building. The penetration loss due to various building material types is incorporated by the *HybridBuildingsPropagationLossModel* class of the *Building* module in NS-3. The penetration loss can also be categorized as wall loss, room loss, floor loss, and building loss from the COST-231 model [35]. The 60 GHz penetration loss for various material types is shown in Table 1 [11].

Table 1. Penetration loss of building materials at 60 GHz.

Material Type (Width)	Penetration Loss (dB)
Granite (3 cm)	30
Glass	1.7 to 4.5
Metalized glass	30
Wooden panels	6.2 to 8.6
Concrete	30
Brick (11 cm)	30

To compare the 60 GHz connectivity with that of the 5 GHz bands we need to model the indoor propagation loss at 5 GHz in the NS-3 modules. The NS-3 *Building* module does not support the metal and glass materials in its building material penetration loss function. To study the reflection and scattering from metal and glass in an indoor environment network performance, we added these material properties to the NS-3 module. As shown in Table 2, the penetration loss was taken into account from the investigation carried out in [36]. The penetration loss from other building materials was supported by the COST-231 model.

Table 2. Penetration loss of building materials at 5 GHz.

Material Type	Penetration Loss (dB)
Wood	4
Concrete with windows	7
Metal	7.1
Stone blocks	12
Concrete without windows	15

5. Performance Evaluation

We conducted a simulation of an automated warehouse using several NS-3 modules to assess the performance of the 60 GHz band within an indoor environment. Our analysis encompassed various network performance metrics, including SINR, mean throughput, and mean delay, across diverse scenarios within the simulated warehouse. Figure 4 illustrates the positions of AMHAs within the warehouse. These positions were strategically chosen to investigate the influence of LOS, nLOS, and dynamic AMHA locations on the 60 GHz network performance. Our evaluation involved scenarios with 1, 2, 5, 7, and 10 AMHAs within the network. We meticulously assessed network performance at various locations within the warehouse, as outlined in Table 3, across a range of case studies. The subsequent subsection presents the results derived from our experimental evaluations.

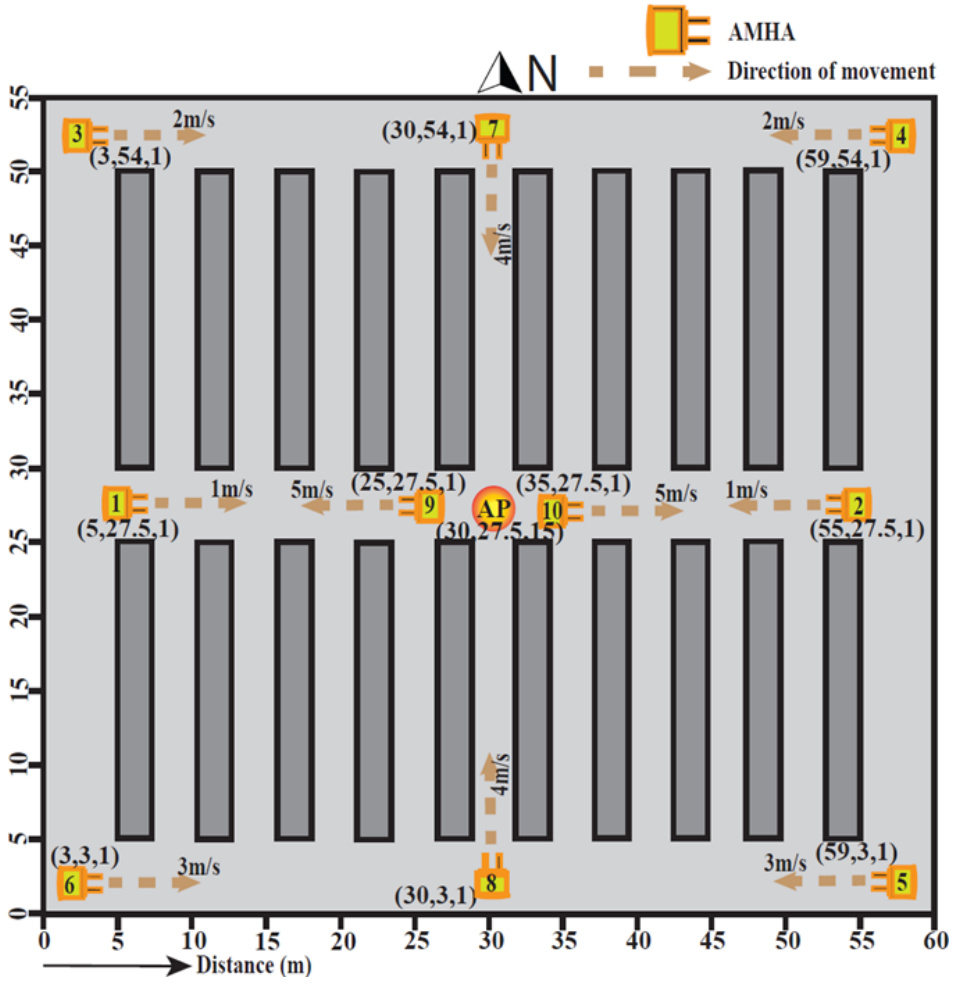

Figure 4. An automated warehouse model is used to analyze the network capacity showing the location of AP and AMHAs (1–10) with their initial positions and directions of movement.

Table 3. Rationale for AMHA positioning.

AMHA Location	Rationale for Positioning
1, 2	East–west path case, to investigate the effects of farthest placed AMHAs with LOS
3, 4, 5, 6	nLOS path case, to investigate the effects of reflective environment with AMHAs farthest from AP
7, 8	North–south path case, to investigate the effect of farther placed AMHAs with LOS within shelf aisles
9, 10	Close proximity case, to investigate the best-case scenario effects

5.1. Throughput and Delay Characteristics of Multiple Cases under Investigation

In this section of the paper, we delve into the multipath environment within an automated warehouse, considering the presence of multiple AMHAs operating at varying total offered loads. The configuration parameters of the automated warehouse, as depicted in Figure 4, are comprehensively detailed in Table 4 [27,37–39]. To enable a thorough exploration of various case scenarios, we strategically position each AMHA within and around the aisles of the automated warehouse, as described in Table 3.

Providing a concise overview of the simulation model parameters, we incorporated numerology, which signifies the subcarrier spacing and slot duration in the physical layer of the 60 GHz wireless communication system. Our performance metrics consist of SINR, which assesses signal quality by comparing the desired signal's strength to unwanted interference and noise, measured as the signal-to-interference and noise power ratio; throughput, quantifying successful data transfer over a specified time frame, expressed in megabits per second (Mbps); and mean delay, which represents the time it takes for the initial bit to traverse the link between the sender and receiver, measured in milliseconds (msec).

Table 4. NS-3 simulated automated warehouse model attributes.

Configuration Parameter	Value
Central Frequency	60 GHz
Bandwidth	100 MHz
Transmission Power	45 dBm
Numerology	5
Modulation Scheme	OFDMA
UDP Packet Size	1000 bytes
Transmitted Packets per Sec.	125,000
AMHA Noise Figure	5.0 dB

5.1.1. Case Study with Stationary AMHAs

In this subsection, we focus on the network's performance in the presence of stationary AMHAs. We conduct a detailed examination of network throughput and delay across various scenarios to assess the significance of LOS paths and multipath components within the automated warehouse. The positions of the AMHAs are strategically chosen based on the criteria outlined in Table 3, allowing us to evaluate the impact of AMHAs at specific locations of interest. Each AMHA's LOS or nLOS relationship with the AP contributes differently to the mean throughput and mean delay per UDP flow within the 60 GHz network, as visually represented in Figures 5 and 6. The position of the AMHA relative to the AP and the presence of LOS or nLOS conditions are pivotal factors influencing the overall performance of the 60 GHz network in an indoor environment. Notably, with only one AMHA in the network, we observed optimal throughput performance, which gradually declined as each additional AMHA was introduced into the warehouse. The

network's performance reached its lowest point when accommodating 7 or 10 AMHAs in the warehouse. This saturation effect occurs at a remarkably low offered load when the maximum number of nodes is present in the warehouse. We observed a similar trend in mean delay, with the 7-AMHA network experiencing a higher delay than the 10-AMHA network. This was partly mitigated by positioning AMHA-9 and AMHA-10 closer to the AP, which compensated for the higher delay observed in the 7-AMHA network. Consequently, the 7-AMHA network exhibited high delay and low throughput performance. For the nLOS-only AMHAs, lower overall SINR values constrained them to operate at lower modulation and coding scheme (MCS) values, resulting in a consistent degradation of both delay and throughput with each additional AMHA. In contrast, AMHA-9 and AMHA-10 enjoyed higher channel quality (SINR) due to short-range LOS signals, allowing them to adopt a higher MCS value of 28. As a result, these links achieved higher individual throughput. Given the consistently short distance between the AP and the AMHA across various positions within the warehouse, the chosen MCS in NS-3 consistently hovered around 26–28. Therefore, the inclusion of AMHA-9 and AMHA-10 led to an overall increase in average throughput and a reduction in average delay within the network. Because throughput and delay vary depending on the AMHAs' positions, we provide a comprehensive overview of channel SINR throughout the entire warehouse as a heatmap in Section 5.4.

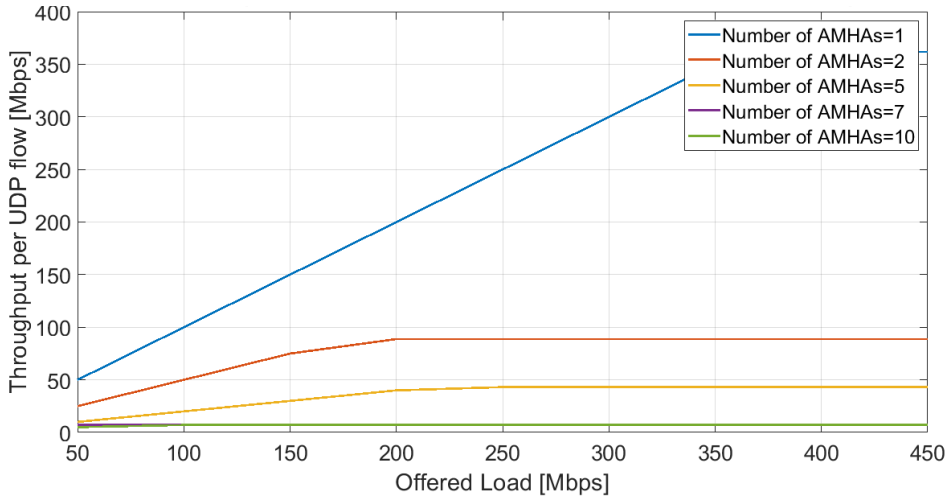

Figure 5. Mean throughput vs. offered load in a stationary AMHA environment.

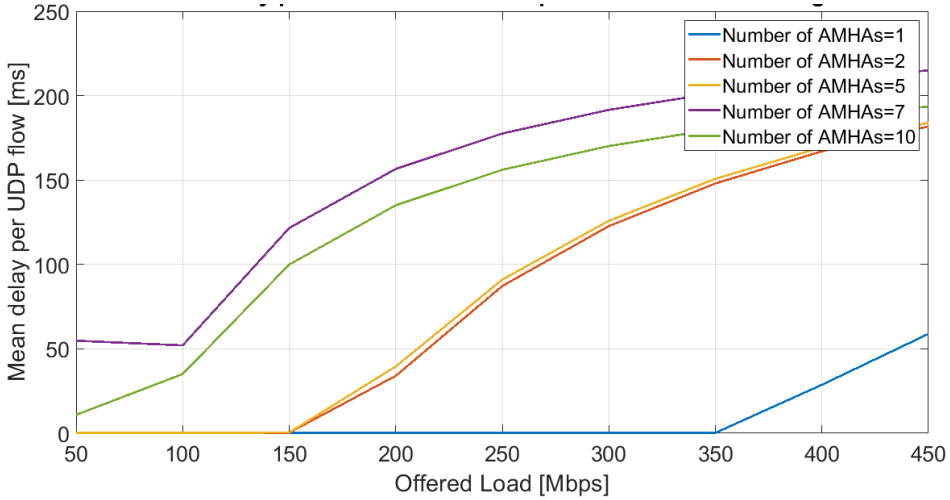

Figure 6. Mean delay vs. offered load in a stationary AMHA environment.

5.1.2. Case Study with Dynamic AMHAs

To replicate a realistic warehouse scenario, we conducted simulations involving mobile AMHAs within a densely populated network. We thoroughly analyzed the performance of the 60 GHz network in the presence of dynamically moving AMHAs, as depicted in Figure 4. Table 3 elucidates the rationale behind our choice of AMHA positions within the warehouse, which allowed us to explore various case studies. For the dynamic AMHAs, we established different operating speeds: AMHA-1 and AMHA-2 moved at 1 m/s, AMHA-3 and AMHA-4 at 2 m/s, AMHA-5 and AMHA-6 at 3 m/s, AMHA-7 and AMHA-8 at 4 m/s, and AMHA-9 and AMHA-10 at 5 m/s within the warehouse. This approach enabled us to thoroughly assess their impact on the performance of the 60 GHz network. Figures 7 and 8 provide insights into the mean throughput and mean delay per UDP flow within the network in the case of dynamic AMHAs. Figures 6 and 8 exhibit a subtle dissimilarity in the average delay between static and dynamic AMHA configurations. This marginal disparity can be attributed to the robust nLOS signals encountered by the AMHA systems. Consequently, the distinction between the static and dynamic AMHA configurations becomes negligible due to the substantial impact of the nLOS conditions.

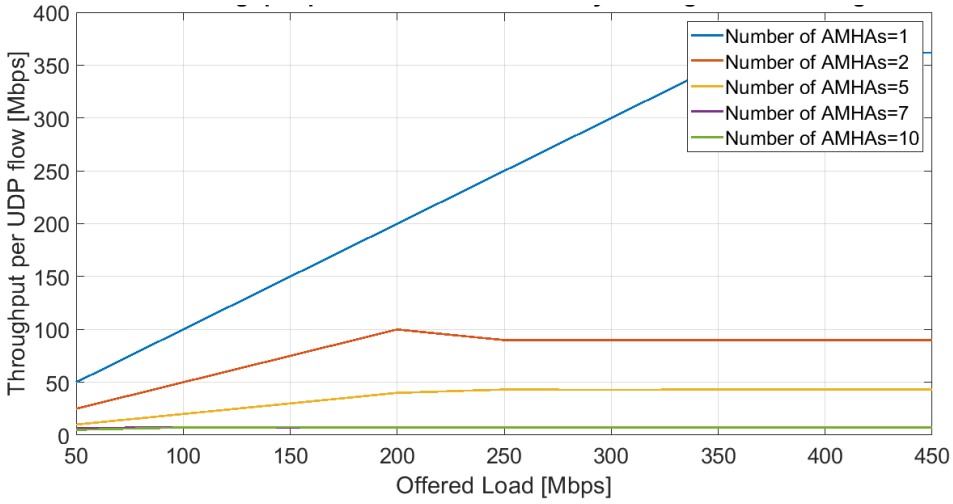

Figure 7. Mean throughput vs. offered load in a dynamic AMHA environment.

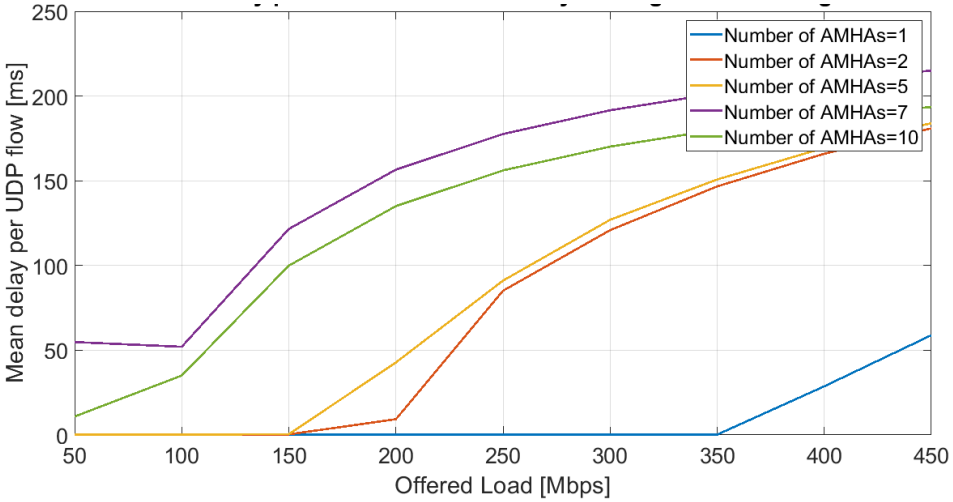

Figure 8. Mean delay vs. offered load in a dynamic AMHA environment.

Within the dynamic warehouse environment, characterized by its limited space for measurements, we observed only marginal improvements in the 60 GHz network's performance under heavy load conditions. This observation aligns with findings presented

in [17]. Remarkably, we found that the speed of the AMHAs had no discernible impact on the automated warehouse network's performance. The mean throughput and mean delay of the network remained consistent with the results from the previous case study in which all AMHAs were stationary. The network reached saturation at a notably high offered load, and it exhibited the lowest mean delay when only 1 or 2 AMHAs were present within the warehouse. Additionally, the positioning of AMHA-9 and AMHA-10 within the warehouse played a significant role in enhancing the network performance when accommodating 10 AMHAs, surpassing the performance of the 7-AMHA scenario. Hence, the specific positions of AMHAs within the warehouse, as well as the presence of LOS or nLOS paths, emerge as critical factors influencing the automated warehouse network's performance. Furthermore, the multipath components proved instrumental in facilitating AMHA movement, even within nLOS scenarios.

5.2. Analyzing SINR Metric for Varying AP Height

In an effort to broaden the scope of our research, we conducted an exploration into the impact of varying the AP heights within the automated warehouse. Specifically, we focused on the LOS-propagated path taken by AMHA-1, as depicted in Figure 1. We conducted this study by maintaining fixed AP heights at 5 m, 10 m, and 15 m. Figure 9 provides a visual representation of the SINR distribution for the LOS path within the indoor warehouse environment, considering different AP heights. Notably, the SINR exhibited a diminishing trend with increasing AP height, especially for short distances. In these scenarios, the LOS links predominated over nLOS links, contributing to this observed decrease in SINR. Furthermore, we observed a gradual SINR reduction with increasing Tx–Rx distance across all cases. In these cases with LOS, the SINR was primarily influenced by the presence of strong LOS signal components. However, as the distances grew larger, it became evident that the LOS power became negligible, and the nLOS power began to dominate the 60 GHz channel model. Consequently, the SINRs in all cases eventually converged to comparable values, primarily determined by the influence of nLOS components.

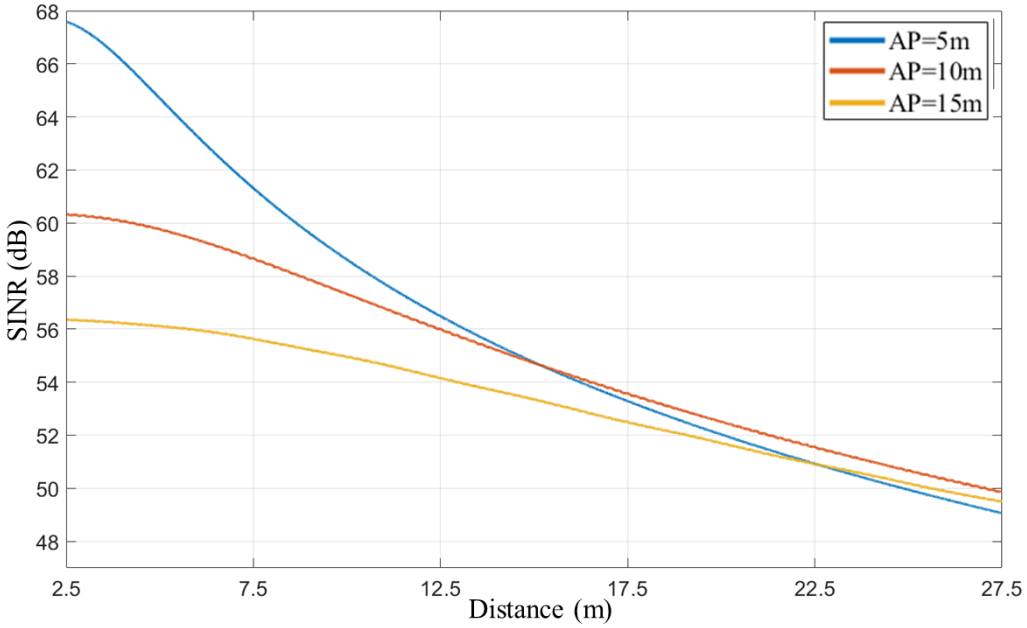

Figure 9. SINR distribution for various AP heights in the LOS case.

We further delved into the examination of how different AP heights influence the 60 GHz network performance within the nLOS scenario. As illustrated in Figure 1, we specifically analyzed the nLOS path taken by AMHA-2, stretching from location C to D. Figure 10 provides an illustrative depiction of the signal-to-interference-plus-noise ratio (SINR) distribution within the nLOS case. Much like the scenarios involving LOS links, we

observed an SINR decrease with an increase in AP height. However, it is worth noting that the presence of metal shelves within the automated warehouse substantially impacted the 60 GHz channel model, leading to a notable dominance of strong reflections. Consequently, the SINR exhibited a slower degradation rate. This observation highlights the significant role played by reflected signals in influencing SINR, particularly as AP heights increased.

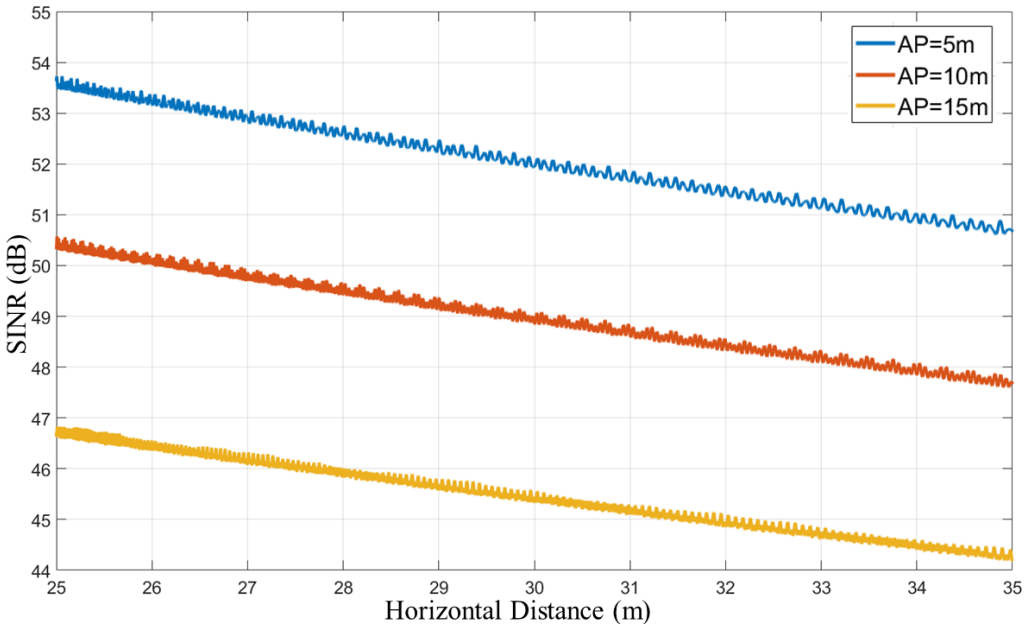

Figure 10. SINR distribution for various AP heights in the nLOS case.

5.3. Analysis of SINR with Different Storage Materials in the Warehouse

Our subsequent investigation centered around evaluating the impact of different storage materials, specifically wood and glass, on the SINR metric. It is noteworthy that at the 60 GHz frequency, the material loss for glass varies from 3.1 to 4 dB, while for wood, it falls within the range of 6.2–8.6 dB, as documented in [11]. Figure 11 provides a visual representation of the 60 GHz indoor network performance within the LOS propagated environment. It is evident that LOS signals primarily dominate wireless connectivity over the initial AMHA–AP distances, regardless of whether the storage environment contains wood or glass. However, a significant difference emerges when examining SINR performance. Due to its lower material loss, the warehouse featuring glass storage outperformed the one with wooden storage materials in terms of SINR. Notably, as the AMHA–AP distance increased, reflected signals began to exert a more substantial influence on SINR performance. This effect manifested in both wood and glass storage environments, leading to a clustering of SINR values in these scenarios.

Subsequently, we turned our attention to the nLOS scenario, wherein we moved AMHA-2 from location C to D at a speed of 5 m/s, as depicted in Figure 1. Within the nLOS context, the SINR was chiefly influenced by the presence of reflected signals within the warehouse. Remarkably, our findings consistently indicated that the presence of glass materials led to superior SINR within the nLOS scenario compared to wood, regardless of the AP's height. This observation is explicitly illustrated in Figure 12.

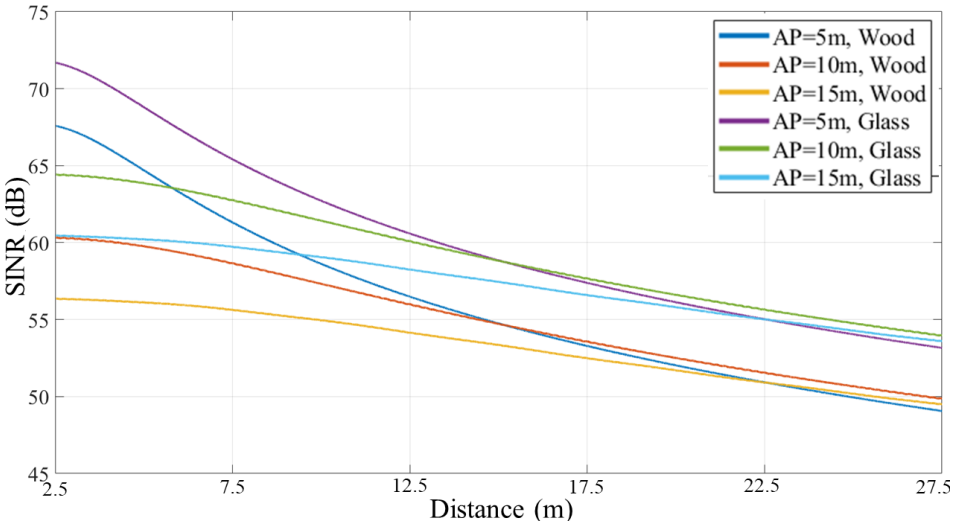

Figure 11. SINR distribution for various AP heights in LOS case.

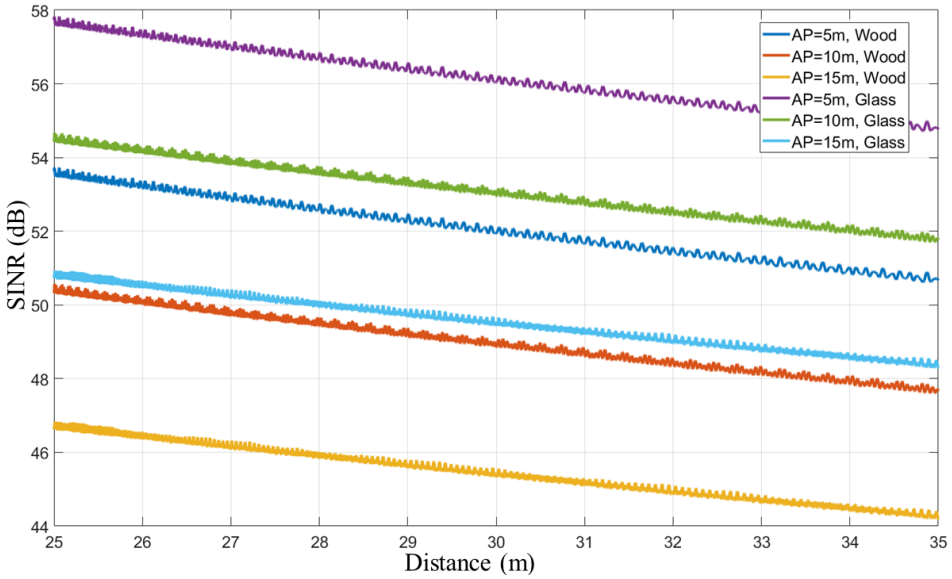

Figure 12. SINR distribution for various AP heights in nLOS case.

5.4. SINR Heatmap

To achieve a deeper insight into the channel conditions across the entire warehouse and to create visual representations of these conditions, we adopted a heatmap technique. In this section, we will illustrate network performance through SINR heatmaps. In these heatmaps, warmer colors highlight regions with strong SINR coverage, whereas cooler colors signify weaker SINR values. These SINR heatmaps are invaluable aids for visualizing the smart warehouse network and evaluating the performance of access points in a densely populated setting.

In our examination of the simulated warehouse, referred to as warehouse model-1 and depicted in Figure 4, we present the SINR distribution for the AP positioned at a height of 15 m, as shown in Figure 13. The AP is located at coordinates (30 m, 27.5 m, 15 m) within the warehouse, using an isotropic antenna system. At this elevation, the influence of LOS signals diminishes in significance, and their presence or absence does not lead to drastic fluctuations. This observation can be attributed to the robust multipath environment generated by the metallic structures present in the warehouse. As the AMHA transitions from the main LOS aisle to the nLOS side aisles, we observe a more gradual SINR shift.

Notably, the SINR reaches its lowest values within the shelving areas due to the presence of metallic boundaries, resulting in significant penetration loss.

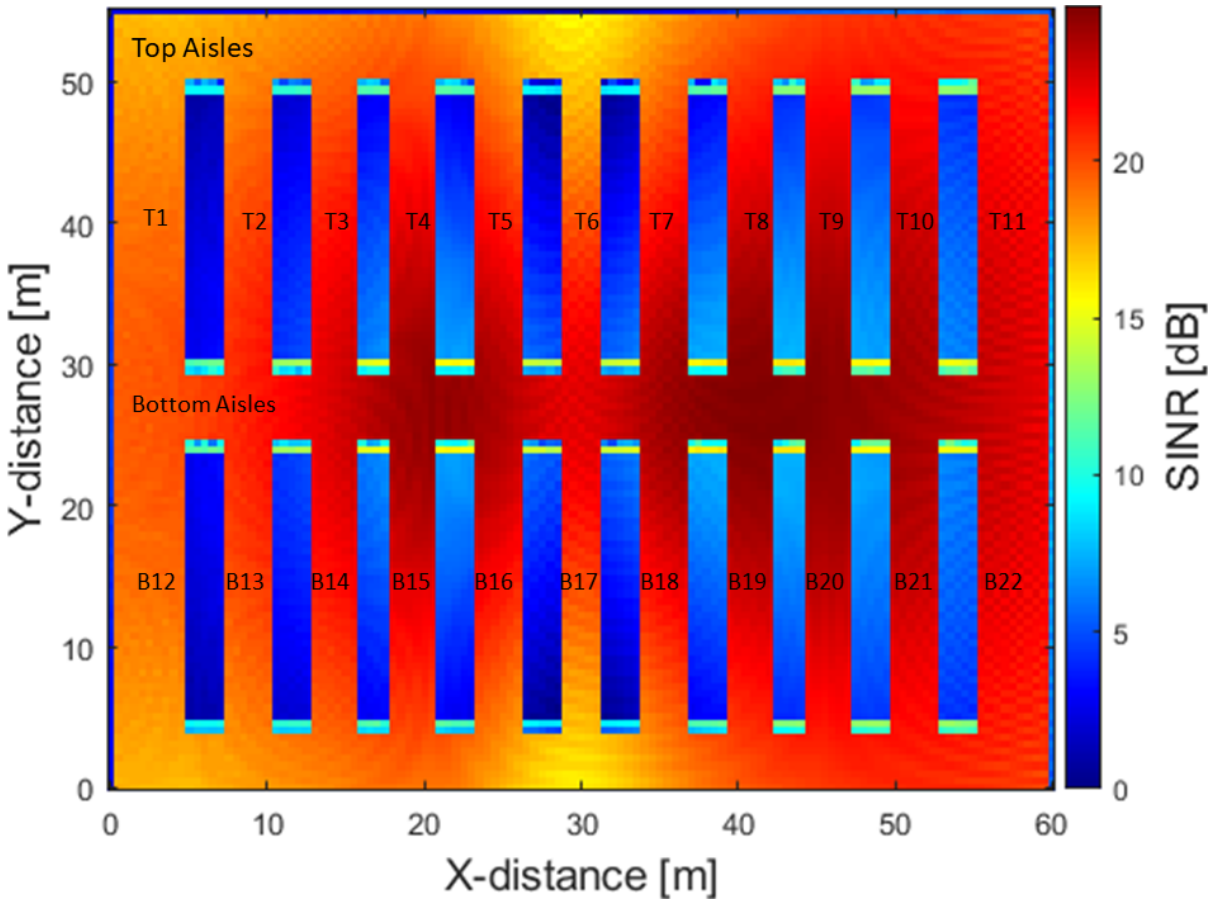

Figure 13. SINR heatmap for warehouse model-1.

Our analysis expanded to assess the 60 GHz network connectivity within a warehouse measuring 60 × 55 × 16 m, as illustrated in Figure 14, denoted as warehouse model-2. In this configuration, the shelving arrangement within the warehouse differed, with clusters of shelves oriented perpendicular to each other. This arrangement represents another common shelving orientation encountered in a warehouse setting. A noteworthy observation was that the shelf locations experienced significant penetration loss, primarily due to the presence of metallic shelves and storage materials. However, in the east-west direction, corresponding to the LOS aisle, we identified an area with strong SINR values. This phenomenon was attributed to the considerable width of the east-west LOS path, measuring 6.5 m. Interestingly, we detected a similarity in the robust signal strength within the nLOS side aisle regions when compared to the nLOS regions in the heatmap featured in Figure 13. The SINR values in these areas displayed a degree of independence from the Tx–Rx distance and were predominantly influenced by the pronounced reflections originating from the metallic shelves.

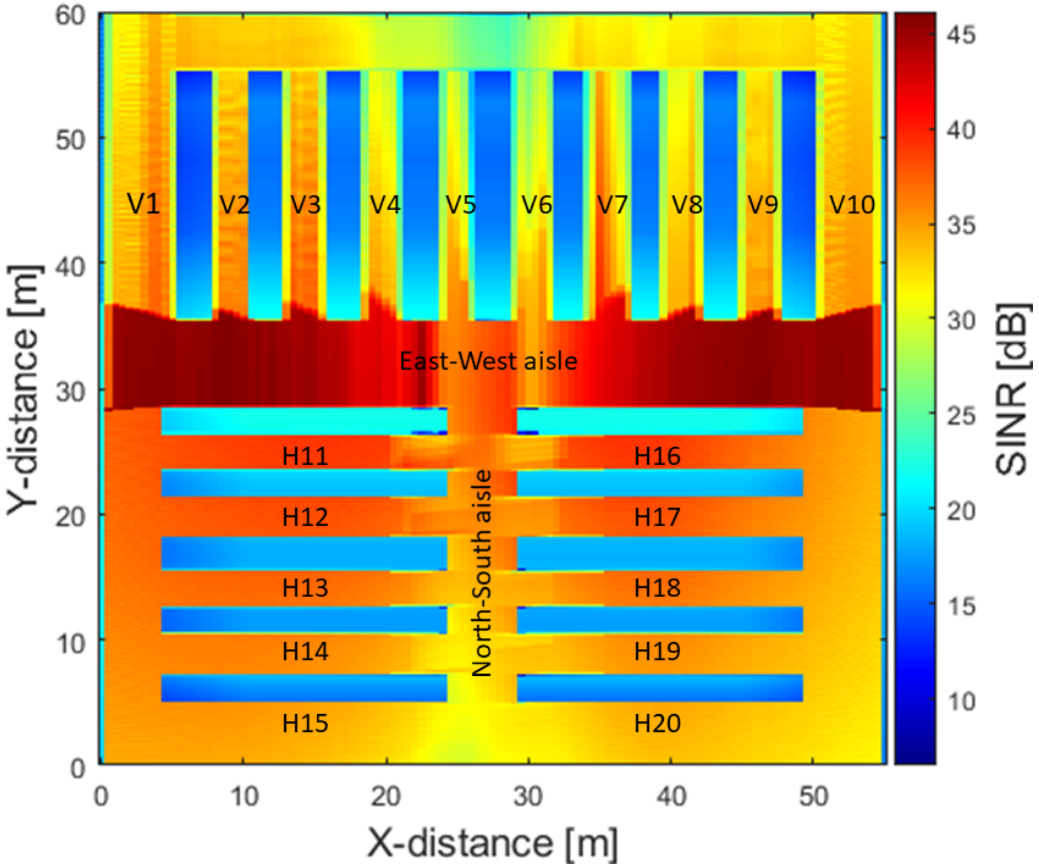

Figure 14. SINR heatmap for warehouse model-2.

5.5. Heatmap Analysis and General Discussion

In this section, we will delve into an in-depth examination of the heatmaps showcased in Figures 13 and 14. Our assessment of the SINR within each aisle has enabled us to establish SINR patterns that apply to various shelf configurations. We have closely examined several critical SINR metrics, encompassing the mean SINR, the standard deviation of the SINR, and the SINR fluctuations as the AMHA moved from the primary LOS aisle (east-west orientation) to any nLOS aisle.

Figure 15 presents a detailed analysis of the SINR within warehouse model-1, as depicted in Figure 13. In this analysis, we will focus on the upper row aisles (aisles 1–11) since the shelf orientation is symmetric in the warehouse. Figure 15a illustrates the mean SINR in each aisle. It is evident that the mean SINR across all aisles falls within the range of 19–23.5 dB, exhibiting variations of less than 5 dB among all the aisles. This observation highlights the potential need for channel compensation in warehouses of this nature when employing 60 GHz band communication. Figure 15b displays the standard deviation in the SINR within each aisle for the entire warehouse. The highest standard deviation of 1.7 dB is observed in the middle aisle (aisle-6). This is attributed to the presence of LOS transmission from the AP into this aisle, resulting in distance-dependent SINR variations within the middle aisles. In contrast, the SINR standard deviation in the nLOS aisles, situated away from the LOS middle aisle, is reduced due to the absence of LOS transmission. SINR in these nLOS aisles depends on multiple reflected multipath transmissions, resulting in a lower correlation between distance within the aisles and SINR. Figure 15c depicts the change or potential discontinuity in the SINR as the automated material handling agent (AMHA) transitions from the main LOS aisle (east–west aisle) into the nLOS aisle. In this figure, we observe an average SINR drop of 0.145 dB. This suggests that the SINR transition into the nLOS aisles does not exhibit significant discontinuities, thereby enabling reliable connectivity within the aisles in this specific warehouse layout.

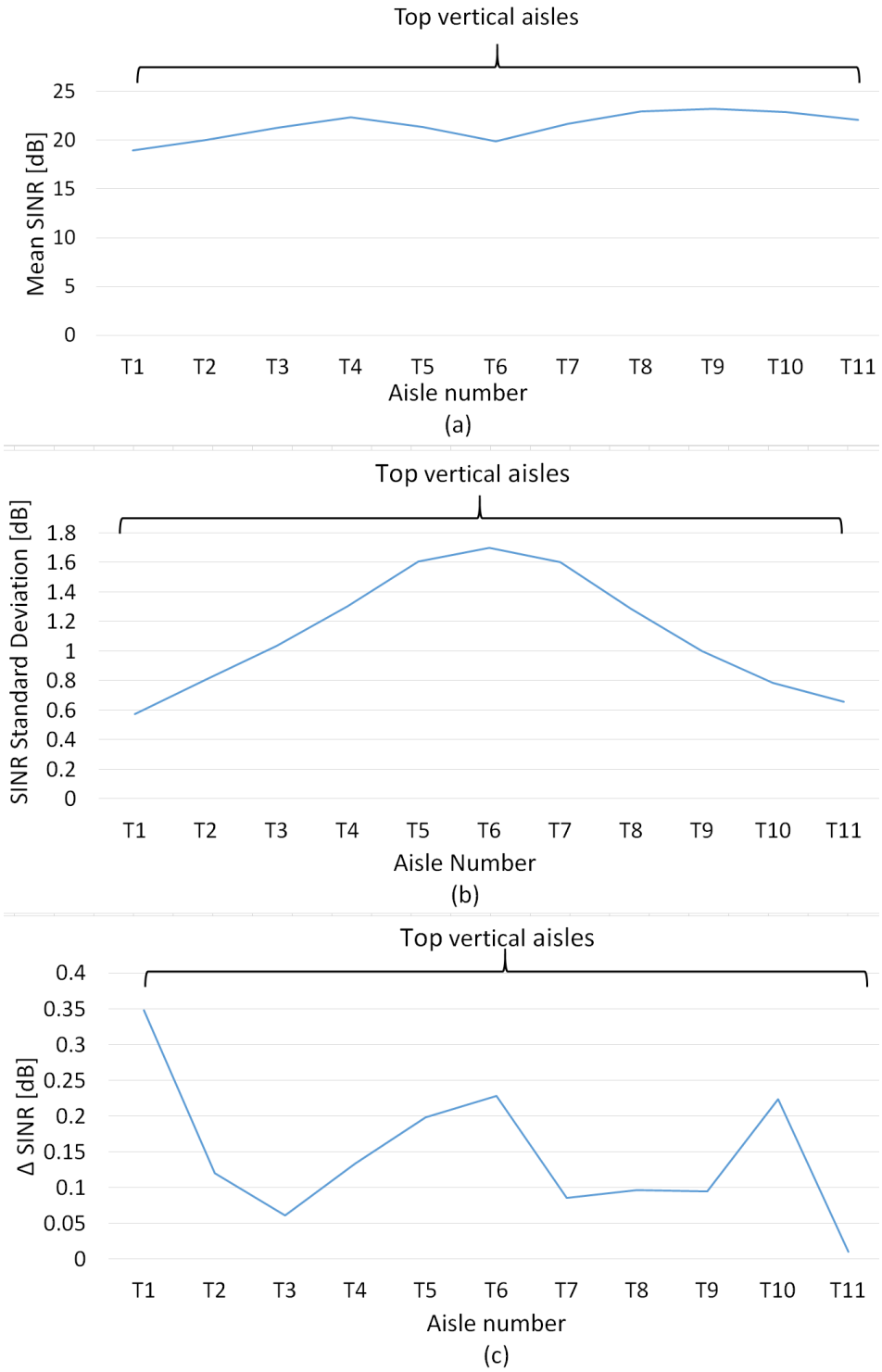

Figure 15. SINR heatmap for warehouse model-1. (**a**) Mean SINR (dB) in each aisle. (**b**) SINR standard deviation (dB) in each aisle. (**c**) Δ SINR (dB) as we move from the main LOS aisle (east–west) to the nLOS aisles (north–south).

Figure 16 provides a detailed analysis of the SINR within warehouse model-2, depicted in Figure 14. The shelf orientation in this configuration differs from warehouse model-1, warranting a close examination of the SINR characteristics. Figure 16a illustrates the mean SINR in each aisle, with values ranging from 29.8 to 38 dB. The mean SINR exhibits variations of less than 8.5 dB among all the aisles. Notably, the overall mean SINR increases across all aisles due to the wider main aisle (east–west), measuring 6.5 m, and a shift in

the aisle configuration. The standard deviation in the SINR within each aisle is depicted in Figure 16b. Aisles V1–V10 exhibit a high standard deviation, averaging 2.8 dB. This is attributed to the relatively wider main aisle (east–west) compared to warehouse model-1 and the presence of strong reflections from the shelves located on the opposite side (shelves of H11 and H16). This results in a large total reflective surface area from the metallic structure, leading to deeper signal penetration into the nLoS aisles and, consequently, a higher standard deviation of the SINR within these aisles. In contrast, the SINR standard deviation in the nLOS aisles H11 to H20 averages 1.3 dB, significantly lower than the upper vertical aisles. This is due to their reduced dependence on LOS signals and the narrower north–south main aisle width. Figure 16c illustrates the change in SINR as the AMHA transitions from the main aisles into the nLOS aisle. In this warehouse configuration, we observe an average SINR drop of 0.7 dB, indicating stable network connectivity in all the aisles.

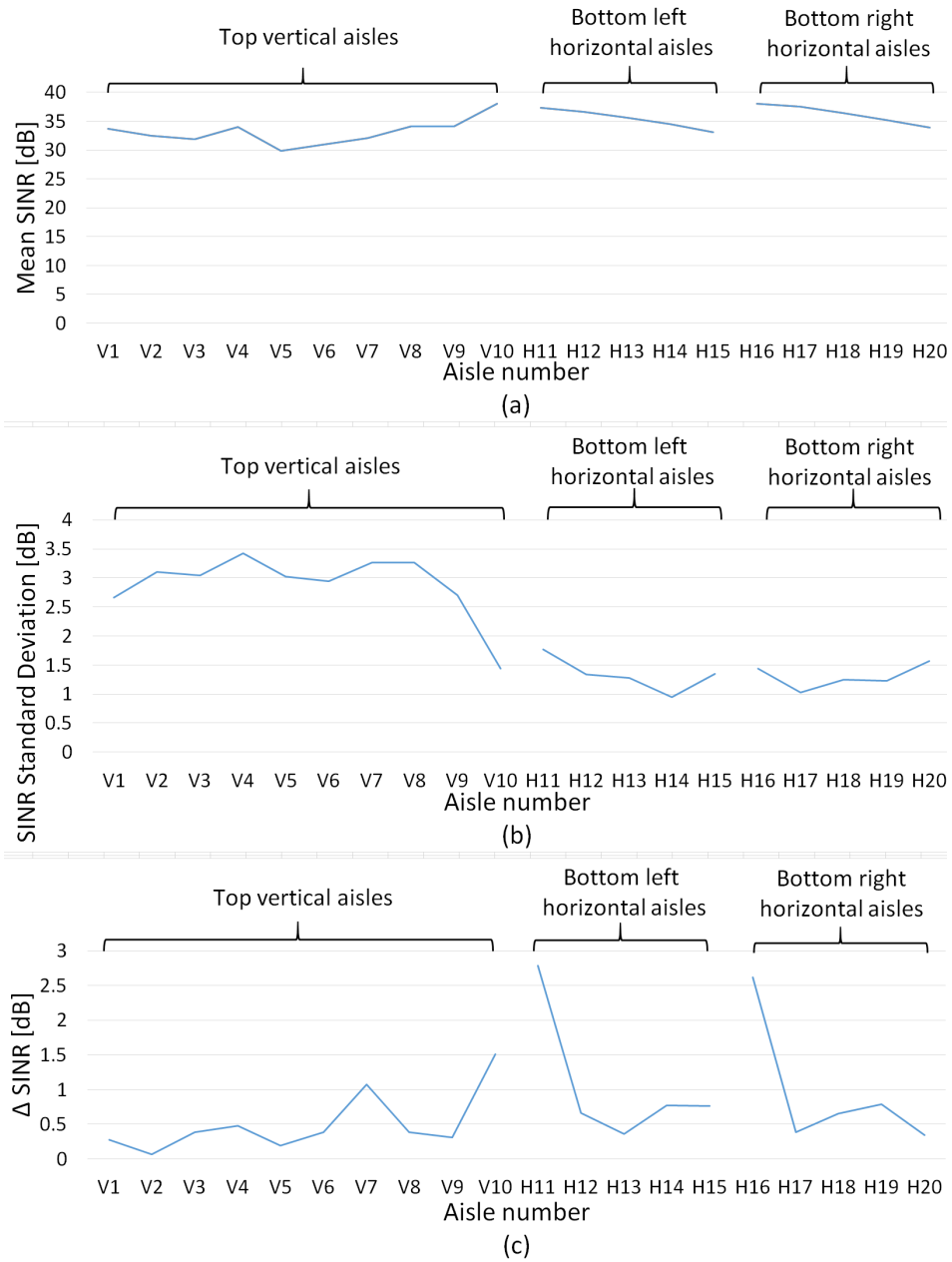

Figure 16. SINR heatmap for warehouse model-2. (**a**) Mean SINR (dB) in each aisle. (**b**) SINR standard deviation (dB) in each aisle. (**c**) Δ SINR (dB) as we move from the main LOS aisle to the nLOS aisles.

Warehouse models 1 and 2 contain typical aisle configurations that are commonly utilized in industrial warehouses, such as the vertical–vertical orientation and the vertical–horizontal orientation. As we switched between the two aisle configurations, we observed a stable 60 GHz network connectivity in both of these warehouse setups—even in a high multipath environment. The mean SINR in Figures 15a and 16a varied within a narrow range (less than 8.5 dB). Both the shelf configurations resulted in a strong multipath environment from the metallic structures in the warehouse, resulting in low standard deviations within each aisle shown in Figures 15b and 16b. Figures 15c and 16c show the change in the SINR as the AMHA moves into the nLOS aisles from the main aisle. Both the figures demonstrate the presence of a stable 60 GHz network in the warehouse models without large discontinuities.

6. Conclusions

We conducted our study in a relatively compact warehouse measuring 60 m $\times$ 55 m. However, warehouses can be much larger, often featuring intricate layouts and shelves arranged irregularly. Consequently, there arises a necessity to delve into network connectivity within each of these distinctive warehouse scenarios, which demands substantial resources. Therefore, a simulation platform like ours can alleviate the need for expensive measurement equipment and enable rapid automation of industry 4.0 systems. In this work, we present a detailed study of the 60 GHz network performance in automated warehouses. The impact of metal shelves was studied to closely monitor the multipath components in a highly dynamic indoor environment. Various channel parameters, such as the SINR, throughput, and delay were analyzed under heavy load in the presence of stationary and dynamic AMHAs. The LOS signals dominate the connection between the AP and the AMHA at shorter distances, however, for longer distances, the nLOS components assist the network performance. It is evident that the multipath components affect the nLOS case scenarios significantly. The presence of metal shelves in an automated warehouse can aid in connectivity of the AMHAs operating in nLOS scenarios and at longer distances. In the presence of multiple AMHAs, we noticed that the network throughput and delay depend on the number of AMHAs in the system as well as their distance from the AP and whether they are in an nLOS-only path or a path with LOS components.

We further investigated the variance in the SINR metric for different AP heights. In an LOS path, the network performance depends on the AP height directly, due to the strong LOS components. The reflected signals played a significant role in the nLOS paths and with an increase in the AP heights. Further, we analyzed the impact of wood and glass storage materials on the network performance and found that glass showed better SINR performance compared to wood due to the low penetration loss for glass material. We presented the SINR heatmaps to analyze the 60 GHz network connectivity in a smart warehouse. We noticed a smooth transition from the LOS aisles to the nLOS aisles. The mean SINR, the standard deviation of the SINR, and the change in SINR when the AMHA moved from the main LOS aisle to any nLOS aisle were closely analyzed for each aisle in the warehouse models under investigation. This demonstrated the presence of a stable 60 GHz network connectivity in the warehouse for multiple shelf configurations. The SINR heatmaps show the variation in the performance of the wireless interconnection at different locations of the warehouse, enabling more efficient warehouse management and automation. In the future, we aim to use a machine learning (ML) approach to analyze network performance with random variations in the shelf storage boxes. We also plan to optimize the number of access points in a given configuration of the warehouse and use the ML model to predict the network performance in potential dead zones and unknown parts of the warehouse for scalability.

This research work is sponsored in part by a grant from The Raymond Corporation. The authors thank Dr. Ehsan Rashidi, Rochester Institute of Technology, for his valuable guidance in the preparation of this paper.

Author Contributions: Conceptualization, R.G. and A.G.; methodology, R.G. and A.G.; software, R.G. and A.V.; validation, R.G., and A.G.; formal analysis, R.G., A.G., C.H., and M.E.K; investigation, R.G., A.G.; resources, A.G. and M.E.K; data curation, R.G.; writing—original draft preparation, R.G.; writing—review and editing, R.G., A.G., C.H., and M.E.K; visualization, R.G., A.G., C.H., and M.E.K ; supervision, A.G.; project administration, M.E.K; funding acquisition, M.E.K. All authors have read and agreed to the published version of the manuscript.

Funding: This research work is sponsored in part by a grant from The Raymond Corporation (RIT Project Number 37272).

Data Availability Statement: The data used in this review paper are generated from publicly available ns3 simulator at https://gitlab.com/nsnam/ns-3-dev (accessed on 31 July 2023). All references and citations are provided in the reference list of this paper. New data were generated and collected for this review.

Acknowledgments: The authors thank Ehsan Rashidi, Rochester Institute of Technology, for his valuable guidance in the preparation of this paper.

Conflicts of Interest: The authors declare no conflict of interest.

Abbreviations

The following abbreviations are used in this manuscript:

2D-DFT	2-Dimensional discrete Fourier transform
3GPP	3rd Generation Partnership Project
AI	Artificial intelligence
AMHA	Autonomous material handling agents
AP	Access point
BS	Base station
DS	Delay spread
EWL	External wall loss
FCC	Federal Communications Commission
HG	Height gain
IOT	Internet of things
IWL	Internal wall loss
LOS	Line of sight
M2M	Machine-to-machine
MCS	Modulation and coding scheme
MIMO	Multiple input multiple output
nLOS	Non-line of sight
NR	New radio
NRP	Normalized received power
NS-3	Network Simulator-3
P2P	Point-to-point
QoS	Quality of service
Rx	Receiver
SCM	Stochastic channel model
SF	Shadow fading
SINR	Signal to interference and noise ratio
U-PA	Uniform planar array
UT	User terminal

References

1. Erboz, G. How To Define Industry 4.0: Main Pillars of Industry 4.0. In *Managerial Trends in the Development of Enterprises in Globalization Era*; Slovak University of Agriculture: Nitra, Slovak, 2017; pp. 761–767 Available online: https://www.researchgate.net/publication/326557388_How_To_Define_Industry_40_Main_Pillars_Of_Industry_40 (accessed on 12 April 2023).
2. Karaman, S.; Frazzoli, E. Sampling-based Algorithms for Optimal Motion Planning. *Int. J. Robot. Res.* **2011**, *30*, 846–894. [CrossRef]
3. Dolgov, D.; Thrun, S.; Montemerlo, M.; Diebel, J. Path Planning for Autonomous Vehicles in Unknown Semi-structured Environments. *Int. J. Robot. Res.* **2010**, *29*, 485–501. [CrossRef]

4. Prakash, C.D.; Akhbari, F.; Karam, L.J. Robust obstacle detection for advanced driver assistance systems using distortions of inverse perspective mapping of a monocular camera. *Robot. Auton. Syst.* **2019**, *114*, 172–186. [CrossRef]
5. Brunetti, A.; Buongiorno, D.; Trotta, G.F.; Bevilacqua, V. Computer vision and deep learning techniques for pedestrian detection and tracking: A survey. *Neurocomputing* **2018**, *300*, 17–33. [CrossRef]
6. Santos, F.; Aquino, A.L.; Madeira, E.R.; Cabral, R.S. Temporal complex networks modeling applied to vehicular ad-hoc networks. *J. Netw. Comput. Appl.* **2021**, *192*, 103168. [CrossRef]
7. Richardson, A.; Watson, P. Use of the 55–65 GHz oxygen absorption band for short-range broadband radio networks with minimal regulatory control. *IEE Proc. (Commun. Speech Vis.)* **1990**, *137*, 233–241. [CrossRef]
8. NR-Physical channels and modulation-Release 15. In *Technical Specification (TS) 38.211*; 3rd Generation Partnership Project (3GPP); Version V15.0.0; 2018. Available online: https://www.etsi.org/deliver/etsi_ts/138200_138299/138215/17.03.00_60/ts_138215v170300p.pdf. (accessed on 13 June 2023)
9. NR and NG-RAN Overall Description-Rel. 15. In *Technical Specification (TS) 38.300*, 3rd Generation Partnership Project (3GPP); Version V15.0.0; 2018. Available online: https://www.etsi.org/deliver/etsi_ts/138300_138399/138300/16.02.00_60/ts_138300v160200p.pdf. (accessed on 13 June 2023)
10. NR-Physical layer measurements-Rel. 15. In *Technical Specification (TS) 38.215*, 3rd Generation Partnership Project (3GPP); Version V15.0.0; 2017. Available online: https://www.etsi.org/deliver/etsi_ts/138300_138399/138300/16.02.00_60/ts_138300v160200p.pdf. (accessed on 13 June 2023)
11. Xu, H.; Kukshya, V.; Rappaport, T. Spatial and temporal characteristics of 60-GHz indoor channels. *IEEE J. Sel. Areas Commun.* **2002**, *20*, 620–630. [CrossRef]
12. Mezzavilla, M.; Zhang, M.; Polese, M.; Ford, R.; Dutta, S.; Rangan, S.; Zorzi, M. End-to-End Simulation of 5G mmWave Networks. *IEEE Commun. Surv. Tutor.* **2018**, *20*, 2237–2263. [CrossRef]
13. Liu, P.; Blumenstein, J.; Perović, N.S.; Di Renzo, M.; Springer, A. Performance of Generalized Spatial Modulation MIMO Over Measured 60GHz Indoor Channels. *IEEE Trans. Commun.* **2018**, *66*, 133–148. [CrossRef]
14. Pitsiladis, G.; Panagopoulos, A.; Constantinou, P. Improving connectivity in indoor millimeter wave wireless networks using diversity reception. In Proceedings of the 6th European Conference on Antennas and Propagation (EUCAP), Prague, Czech Republic, 2012; pp. 510–514. [CrossRef]
15. Fan, D.; Gao, F.; Wang, G.; Zhong, Z. A 2D-DFT Based Channel Estimation Scheme in Indoor 60GHz Communication Systems with Large-Scale Multiple-Antenna. In Proceedings of the 2016 IEEE 83rd Vehicular Technology Conference (VTC Spring), Nanjing, China, 15–18 May 2016; pp. 1–5. [CrossRef]
16. Arya, P.; Huang, L.Y.; Liu, W.C.; Chang, H.T.; Jen, C.W.; Wu, C.F.; Jou, S.J. Gb/s prototyping of 60GHz indoor wireless SC/OFDM transmitter and receiver on FPGA demo system. In Proceedings of the 2015 IEEE International Conference on Consumer Electronics-Taiwan, Taipei, Taiwan, 6–8 June 2015; pp. 204–205. [CrossRef]
17. Gulia, R.S.; Mamun, S.A.; Vashist, A.; Ganguly, A.; Hochgraf, C.; Kwasinski, A.; Kuhl, M.E. Evaluation of Wireless Connectivity in an Automated Warehouse at 60 GHz. In Proceedings of the 2022 IEEE International Conference on Consumer Electronics (ICCE), Las Vegas, NV, USA, 7–9 January 2022; pp. 1–6. [CrossRef]
18. Karaagac, A.; Haxhibeqiri, J.; Joseph, W.; Moerman, I.; Hoebeke, J. Wireless industrial communication for connected shuttle systems in warehouses. In Proceedings of the 2017 IEEE 13th International Workshop on Factory Communication Systems (WFCS), Trondheim, Norway, 31 May–2 June 2017; pp. 1–4. [CrossRef]
19. Yang, J.; Ai, B.; You, I.; Imran, M.; Wang, L.; Guan, K.; He, D.; Zhong, Z.; Keusgen, W. Ultra-Reliable Communications for Industrial Internet of Things: Design Considerations and Channel Modeling. *IEEE Netw.* **2019**, *33*, 104–111. [CrossRef]
20. Li, S.; Liu, Y.; Lin, L.; Sun, D.; Yang, S.; Sun, X. Simulation and Modeling of Millimeter-Wave Channel at 60 GHz in Indoor Environment for 5G Wireless Communication System. In Proceedings of the 2018 IEEE International Conference on Computational Electromagnetics (ICCEM), Chengdu, China, 26–28 March 2018; pp. 1–3. [CrossRef]
21. Hajj, M.E.; El Zein, G.; Zaharia, G.; Farhat, H.; Sadek, S. Angular Measurements and Analysis of the Indoor Propagation Channel at 60 GHz. In Proceedings of the 2019 International Conference on Wireless and Mobile Computing, Networking and Communications (WiMob), Barcelona, Spain, 21–23 October 2019; pp. 121–126. [CrossRef]
22. Kacou, M.; Guillet, V.; El Zein, G.; Zaharia, G. Coverage and Throughput Analysis at 60 GHz for Indoor WLAN with Indirect Paths. In Proceedings of the 2018 IEEE 29th Annual International Symposium on Personal, Indoor and Mobile Radio Communications (PIMRC), Bologna, Italy, 9–12 September 2018; pp. 1–5. [CrossRef]
23. Zekri, A.B.; Ajgou, R.; Chemsa, A.; Ghendir, S. Analysis of Outdoor to Indoor Penetration Loss for mmWave Channels. In Proceedings of the 2020 1st International Conference on Communications, Control Systems and Signal Processing (CCSSP), El Oued, Algeria, 29 July 2020; pp. 74–79. [CrossRef]
24. Jun, S.Y.; Caudill, D.; Chuang, J.; Papazian, P.B.; Bodi, A.; Gentile, C.; Senic, J.; Golmie, N. Penetration Loss at 60 GHz for Indoor-to-Indoor and Outdoor-to-Indoor Mobile Scenarios. In Proceedings of the 2020 14th European Conference on Antennas and Propagation (EuCAP), Copenhagen, Denmark, 15–20 March 2020; pp. 1–5. [CrossRef]
25. Shkel, A.; Mehrabani, A.; Kusuma, J. A Configurable 60GHz Phased Array Platform for Multi-Link mmWave Channel Characterization. In Proceedings of the 2021 IEEE International Conference on Communications Workshops (ICC Workshops), Montreal, QC, Canada, 14–23 June 2021; pp. 1–6. [CrossRef]

26. Bakirtzis, S.; Chen, J.; Qiu, K.; Zhang, J.; Wassell, I. EM DeepRay: An Expedient, Generalizable, and Realistic Data-Driven Indoor Propagation Model. *IEEE Trans. Antennas Propag.* **2022**, *70*, 4140–4154. [CrossRef]
27. Vashist, A.; Bhanushali, D.R.; Relyea, R.; Hochgraf, C.; Ganguly, A.; Sai Manoj, P.D.; Ptucha, R.; Kwasinski, A.; Kuhl, M.E. Indoor Wireless Localization Using Consumer-Grade 60 GHz Equipment with Machine Learning for Intelligent Material Handling. In Proceedings of the 2020 IEEE International Conference on Consumer Electronics (ICCE), Las Vegas, NV, USA, 4–6 January 2020; pp. 1–6. [CrossRef]
28. Cheema, S.; Sepehri, N. Computer aided stability and safety analysis of forklifts. In Proceedings of the 5th Biannual World Automation Congress, Orlando, FL, USA, 9–13 June 2002; Volume 14, pp. 297 – 302. [CrossRef]
29. 3GPP. Study on Channel Model for Frequencies from 0.5 to 100 GHz. In *Technical Specification (TS) 38.901*; 3rd Generation Partnership Project (3GPP), Version V15.0.0, 2019. Available online: https://www.etsi.org/deliver/etsi_tr/138900_138999/138901/16.01.00_60/tr_138901v160100p.pdf (accessed on 13 June 2023).
30. Zugno, T.; Polese, M.; Patriciello, N.; Bojović, B.; Lagen, S.; Zorzi, M. Implementation of a Spatial Channel Model for ns-3. In Proceedings of the 2020 Workshop on ns-3. ACM, Gaithersburg, MD, USA, 17–18 June 2020. [CrossRef]
31. Larranaga, A.; Lucas-Estan, M.C.; Lagen, S.; Ali, Z.; Martinez, I.; GoZalvez, J. An open-source implementation and validation of 5G NR configured grant for URLLC in ns-3 5G LENA: A scheduling case study in industry 4.0 scenarios. *J. Netw. Comput. Appl.* **2023**, *215*. [CrossRef]
32. Maltsev, A.; Maslennikov, R.; Sevastyanov, A.; Lomayev, A.; Khoryaev, A. Statistical channel model for 60 GHz WLAN systems in conference room environment. In Proceedings of the Fourth European Conference on Antennas and Propagation, Barcelona, Spain, 12–16 April 2010; pp. 1–5.
33. Yang, H.; Herben, M.; Smulders, P. Impact of antenna pattern and reflective environment on 60 GHz indoor radio channel characteristics. *IEEE Antennas Wirel. Propag. Lett.* **2005**, *4*, 300–303. [CrossRef]
34. Cassioli, D.; Win, M.; Molisch, A. The ultra-wide bandwidth indoor channel: From statistical model to simulations. *IEEE J. Sel. Areas Commun.* **2002**, *20*, 1247–1257. [CrossRef]
35. Mogensen, P.E.; Wigard, J. *COST Action 231: Digital Mobile Radio towards Future Generation Systems: Final Report*; Publications Office of EU: Luxembourg, 1999.
36. Lott, M.; Forkel, I. A multi-wall-and-floor model for indoor radio propagation. In Proceedings of the IEEE VTS 53rd Vehicular Technology Conference, Spring 2001. Proceedings (Cat. No.01CH37202), Rhodes, Greece, 6–9 May 2001; Volume 1, pp. 464–468. [CrossRef]
37. Kodak, U.; Rupakula, B.; Zihir, S.; Rebeiz, G.M. A 62 GHz Tx/Rx 2x128-Element Dual-Polarized Dual-Beam Wafer-Scale Phased-Array Transceiver with Minimal Reticle-to-Reticle Stitching. In Proceedings of the 2019 IEEE Radio Frequency Integrated Circuits Symposium (RFIC), Boston, MA, USA, 2–4 June 2019; pp. 335–338. [CrossRef]
38. Hakem, N.; Delisle, G.; Coulibaly, Y. Radio-wave propagation into an underground mine environment at 2.4 GHz, 5.8 GHz and 60 GHz. In Proceedings of the The 8th European Conference on Antennas and Propagation (EuCAP 2014), Hague, The Netherlands, 6–11 April 2014; pp. 3592–3595. [CrossRef]
39. Ramos, A.R.; Silva, B.C.; Lourenço, M.S.; Teixeira, E.B.; Velez, F.J. Mapping between Average SINR and Supported Throughput in 5G New Radio Small Cell Networks. In Proceedings of the 2019 22nd International Symposium on Wireless Personal Multimedia Communications (WPMC), Lisbon, Portugal, 24–27 November 2019; pp. 1–6. [CrossRef]